International Journal of Computational and Experimental Science and ENgineering
(IJCESEN)
Vol. 11-No.3 (2025) pp. 5552-5558
http://www.ijcesen.com
ISSN: 2149-9144

Research Article

Optimizing T1-Weighted MRI Image Quality: A Comparative Study In Two Acquisition Protocols In Lumbar Spine Imaging

Amna Saeed Qaeed [1*], Mawada M. Funjan[2], Maryam Issa Al-Ani[3]

[1]Department of Physiology, College of Medicine, University of Baghdad, Baghdad, Iraq.
* **Corresponding Author Email** : Aamna.Qaed2308m@comed.uobaghdad.edu.iq- **ORCID:** 0000-0002-5247-3850

[2]Department of Physiology, College of Medicine, University of Baghdad, Baghdad, Iraq.
Email: mawadamousa@comed.uobaghdad.edu.iq- **ORCID:** 0000-0002-5247-3250

[3]Department of Surgery, College of Medicine, University of Baghdad, Baghdad, Iraq.
Email: Mariam.i@comed.upbaghdad.edu.iq- **ORCID:** 0000-0002-5247-3350

Article Info:

DOI: 10.22399/ijcesen.3517
Received : 21 May 2025
Accepted : 18 July 2025

Keywords

T1-Weighted MRI Image Quality
Two Acquisition Protocols
Lumbar Spine Imaging

Abstract:

Objective: To assess the effect of different acquisition parameters on the quality of T1-weighted sagittal lumbar spine MRI images using manual measurements, automated quantitative analysis, and expert visual assessment.

Materials and Methods

This was a cross-sectional study of 200 lumbar MRI scans performed with a 1.5T Siemens Avanto. Two T1-Weighted imaging protocols that differed in TR, matrix size, slice thickness, FOV read, and number of slices. Objective image quality metrics, signal-to-noise ratio (SNR), contrast-to-noise ratio (CNR), edge strength, Laplacian variance, and entropy, were obtained. using manual measurement for ROIs, and automatic measurement using image processing (Python). Statistical comparisons were conducted using SPSS with a significance level of $p<0.05$.

Results

The second protocol (shorter TR, larger voxel size, lower spatial resolution) had a significantly higher signal-to-noise ratio (SNR) and contrast-to-noise ratio (CNR). On the other hand, a better edge strength was obtained with the first Protocol (longer TR, higher resolution, smaller voxels); however, Laplacian variance and entropy showed no statistical difference. Visual assessment by a radiologist preferred the first protocol for tissue contrast, though both protocols were clinically acceptable.

Conclusion

An optimal MRI acquisition parameter, particularly TR, spatial resolution, and voxel size, improves the quality of T1-weighted images in the lumbar spine. These results may encourage optimization of protocols to balance image quality and scan efficiency.

1. Introduction

Magnetic resonance imaging (MRI) is one of the most widely used diagnostic tools in medical imaging [1]. It is a non-invasive technique [2] that provides detailed, high-resolution anatomical images of the internal structures of the human body. One of its major advantages is the use of magnetic field instead of ionizing radiation [3], MRI is highly effective in differentiate between various types of tissue [4] and fluids depending on their signal intensity characteristics [5] additionally, it is less affected by the artifact that produces from the bones [6] MRI is based on using a magnetic field, which interacts with the rotational properties of hydrogen atoms in water molecules, which comprise 80% of the human body's composition [7].

MRI images is created by applying a radiofrequency pulse(RF), followed by signal generation through resonance phenomenon, longitudinal and transverse relaxation mechanisms, and free inductive decay signals, which all contribute to the resulting image contrast. [8].

The Pulse sequences are computer programs that are used to encode the strength and timing of radiofrequency pulses(RF) and gradient fields to acquire image data. Common sequences includes fast spin echo (FSE), gradient echo (GRE), steadystate free precession (SSFP), and echo planar imaging (EPI) [9] In this study, two T1-weighted imaging protocols using fast spin echo sequences are compared.

Each MRI sequence is defined by several parameters, including repetition time (TR) which is defined as the time between two successive RF pulses applied at the same part of the tissue and its measured in milliseconds (ms), Echo time (TE) it is defined as the time interval between applied radiofrequency pulse and the peak of the signal is measured in milliseconds (ms) [10]

The matrix size in magnetic resonance imaging (MRI) refers to the number of pixels that make up a two-dimensional image. It is represented as rows × columns (e.g., 256 × 256) [11].

The Slice thickness refers to the depth of the image captured during the scan, and it determines the amount of anatomical information recorded in the z-axis. the number of slices refers to the cross-sectional images collected in a single scan time to cover a specific anatomical region, and it determines the volume of tissue scanned in the slice-selection (Z) direction [12]. These parameters collectively determine the voxel size, which is the smallest unit of three-dimensional spatial information in MRI images voxel size has an important role in image quality as larger the voxel size it improves the SNR by averaging signals and smaller voxel size improves the spatial resolution but degrades SNR [20].

These acquisition parameters significantly influence both the image quality and scan time, the image quality can be assessed by using objective metrics such as signal to noise ratio (SNR) and contrast-noise ratio (CNR). SNR can be defined as the ratio of the mean of signal intensity of the region of interest (ROI) to the standard deviation of the noise in the background [14] and can be given by the equation:

$$SNR = \frac{mean\ signal\ of\ ROI}{standard\ devition\ of\ background\ noise} \qquad (14)$$

CNR can be defined as the difference between the mean of signal intensity of two different regions of interest (ROI) divided by the standard devotion of the noise in the background (8), and can be given by the equation:

$$CNR = \frac{mean\ signal\ of\ ROI1 - mean\ signal\ of\ ROI2}{standard\ devition\ of\ background\ noise} \qquad (8)$$

Additional metrics include edge strength, which quantifies the intensity gradient between pixels and it reflects anatomical sharpness and clarity [15], Laplace -variance, which measures image sharpness by evaluating high-frequency content A higher contrast usually means that the image has better focus and more texture information [16]; and entropy is a statistical measure of randomness that indicates the complexity, higher entropy indicates richer tissue detail and tissue contrast [18] this study aims to assess the impact of varying acquisition parameters on the quality of T1-weighted sagittal lumber spine Images by combining manual ROI measurements, automated analysis using python-based image processing, and a radiologist visual assessment.

2. Material and Methods

This cross-sectional study was carried out in two different centers within 6 months (October 2024 to March 2025) on the same 1.5T Siemens Avanto MRI scan. A total of 234 patient cases were reviewed the mean ages of 43±9.6. A 200 cases (112 females and 88 males) were enrolled following the exclusion criteria of scoliosis, partial imaging, or incomplete demographic data. Sagittal T1-weighted lumbar spine sequences were obtained using two different protocols differing in TR, matrix, slice thickness, FOV read, and number of slices, Table 1. shows the acquisition parameters for both protocols

Table 1. *MRI acquisition parameters for both protocols*

Parameters	First protocol	Second protocol
Repetition time (TR)(ms)	834	450
Matrix	384*288	256*154
Slice thickness(mm)	4	4.5
FOV read	335	420
Number of slices	13	10

The reliability of the images was rated in three stages:

Manual ROIs measurement assessment:

Signal-to-noise ratio (SNR) and contrast-to-noise ratio (CNR) were measured on RadiAnt DICOM viewer using regions of interest (ROIs) that were manually drawn in the vertebral body (for signal), cerebrospinal fluid (CSF) (for contrast), and air background area (for noise). Each ROI contained ~80 pixels as in figures 1 and 2. The mean signal intensity and SD for the noise were recorded. Voxel size (mm3) was calculated using the parameters obtained from the radiant DICOM, following the equation:

$$voxel\ size\ = \frac{FOVx}{Number\ of\ pixels\ X} * \frac{FOV\ y}{Number\ of\ pixel\ Y} * slice\ thickness\ Z \qquad (20)$$

Where:

FOVx: field of view in the read direction (FOV read) in mm
Pixel number x: is the number of pixels in the read direction (eg for a matrix of 384*288, the 384 is the number of pixels in the read direction)
FOV y: Field of view in the phase direction (FOV phase) [mm]
Number of pixels y: The number of pixels in the phase direction, for example, if the matrix size is 384*288, the 288 is the number of pixels in the phase direction.
Z Slice thickness: the thickness of the slice in mm or the Z-direction.

Figure 1. *Shows ROIs in the first protocol in T1-weighted*

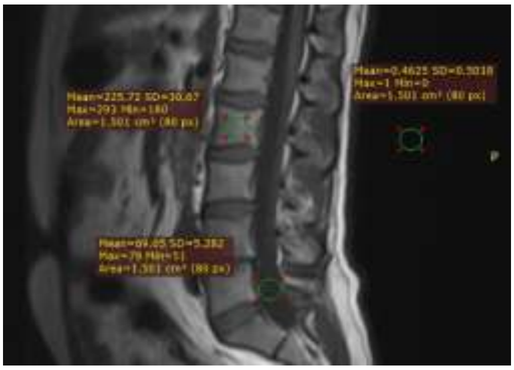

Figure 2. *Shows the ROIs for the second protocol in T1-weighted.*

Automated Image Processing Analysis

An automatic image reader was generated: (Python NumPy, OpenCV, Scikit-Image) to calculate automatic image quality metrics. As in Figure 3., the MRI images were exported in lossless PNG format and then transformed to grayscale. Binary masks were then applied to define regions of interest (ROIs) in the vertebral body and CSF, and to exclude surrounding tissues. The signal ROI was located inside the vertebral body, and the CSF provided contrast area for CNR measurement. Background noise was measured in a homogeneous air region outside of the patient's body. Each ROI was defined using binary masks (1 = ROI, 0 = background) and allowed for pixel-based extraction of the values. From these regions, the script calculated the following quality measures: Signal-to-Noise Ratio (SNR), CNR (Contrast-to-Noise Ratio), EdgeStrength, Laplacian Variance, and Entropy.

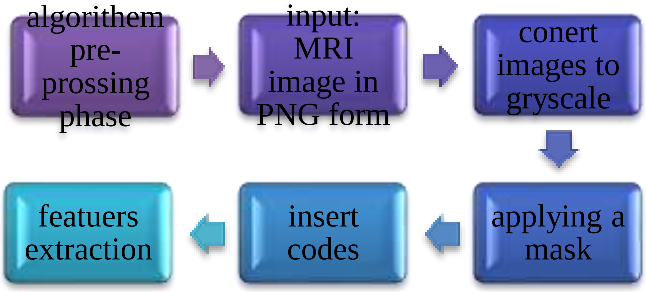

Figure 3. *Workflow for MRI image preprocessing and feature extraction using python*

Visual assessment by a radiologist

The quantitative analysis was complemented by a subjective evaluation of image quality by an experienced radiologist on a structured-questionnaire basis. This assessment was performed by blinded image set reviews for images from T1-weighted sequences obtained using two different protocols. The Radiologist rated each image independently.

Statistical Analysis

All quality image data were analyzed with SPSS (version 26). Continuous variables were summarized by means and standard deviations. Normality was checked by the Kolmogorov–Smirnov test, and the normality was confirmed, so the parametric tests could be employed. An independent sample T-test was used for quantitative comparison, and categorical visual score comparison was conducted with Chi-square test. Values of $p < 0.05$ were considered to be statistically significant.

3. Result

On vertebral level, the manual measurements showed significant differences in signal-to-noise ratio (SNR) and contrast-to-noise ratio (CNR) between the two protocols. In the vertebral body, the first protocol resulted in a mean SNR of 70.69 ± 29.28 while the second protocol provided a significantly higher SNR of 552.45 ± 314.97 ($p < 0.001$). The mean SNR for CSF using the first and second protocols was 32.29 ± 16.44 and 186.31 ± 118.87, respectively ($p < 0.001$), table 2. For CNR, protocol 1 obtained a mean value of 38.40 ± 25.28, while in protocol 2 the mean was significantly higher at 306.65 ± 190.31 ($p < 0.001$), table 3. These results demonstrate a stable and statistically significant enhancement of the signal and contrast characteristics of the second imaging protocol. The calculated voxel sizes were 1.21 mm^3 for the first Protocol and 4.79 mm^3 for the second Protocol. These differences are a product of the resolution matrix, field of view (FOV), and slice thickness used in the two protocols.

Trends were similar when assessed with automated image quality analysis. Table 4. shows that the SNR (1.15 ± 0.14) and CNR (5.43 ± 0.48) of the second protocol were significantly higher when compared to the first protocol (SNR = 1.01 ± 0.13; CNR = 4.87 ± 0.41) in both cases ($p < 0.001$). Edge strength was additionally greater within the first protocol (7.44 ± 0.79 versus 5.74 ± 0.71, $p < 0.001$). However, Laplacian variance (328.63 ± 48.55 vs. 322.03 ± 93.24, $p = 0.475$) and entropy (3.11 ± 0.39 vs. 3.14 ± 0.19, $p = 0.444$) did not differ significantly between the two groups. These findings indicate that the first and second protocols gave similar levels of image texture and complexity, although the former protocol resulted in a higher edge sharpness and contrast. Radiologist's visual assessment also supported the interpretation of image quality variations. Anatomical clarity and acquisition time were rated (good), and they were equivalent between the two protocols, but the first protocol received a higher rating for tissue contrast (sharp) relative to the second Protocol (moderate). This is consistent with the edge strength and contrast measures. The first protocol acquisitions were 6.53 minutes long against 4 minutes long for the second protocol, supporting the good practical efficiency of the second protocol with a minor loss in the visual quality.

Table 2. *Independent sample T-test between T1-weighted protocols and signal to noise ratio (SNR) using manual ROIs measurement*

(ROI)	Protocol	SNR		Significance
		Mean	SD	
Vertebra 80	First	70.69	29.28	p- value < 0.001
	second	552.45	314.97	
CSF 80	First	32.29	16.44	p- value < 0.001
	second	186.31	118.87	

Table 3. *Independent sample T-test between T1-weighted protocols and signal to noise ratio (CNR) using manual ROIs measurement*

Protocol type	CNR		Significance
	Mean	SD	
First protocol	38.40	25.28	p- value < 0.001
Second protocol	306.65	190.31	p- value < 0.001

Table 4. *Independent sample T-test between T1-weighted protocols and SNR, CNR, Edge-strength, Laplacian-var, and entropy using Automated Image Processing Analysis*

	Protocol	**mean**	**SD**	**Significance**
SNR	First	1.01	0.13	p- value < 0.001
	Second	1.15	0.14	
CNR	First	4.87	0.41	p- value < 0.001
	Second	5.43	0.48	
Edge_ Strength	First	7.44	0.79	p- value < 0.001
	Second	5.74	0.71	
Laplacian_ Var	First	328.63	48.55	p- value = 0.475
	Second	322.03	93.24	
Entropy	First	3.11	0.39	p- value = 0.444
	Second	3.14	0.19	

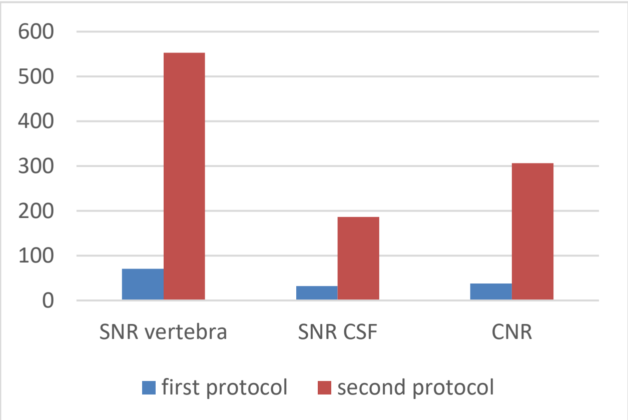

Figure 4. *Mean values of SNR and CNR using Manual ROIs measurement.*

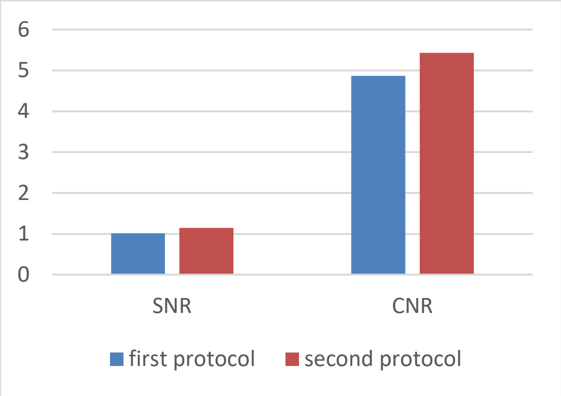

Figure 5. *Mean values of SNR and CNR using Automated Image Processing Analysis*

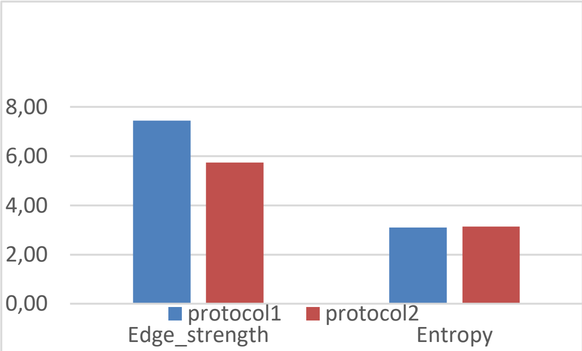

Figure 6. *Mean values of edge-strength and entropy using Automated Image Processing Analysis*

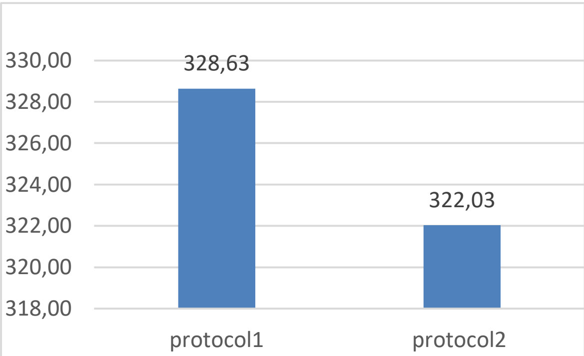

Figure 7. *Mean values of Laplacian-var using Automated Image Processing Analysis*

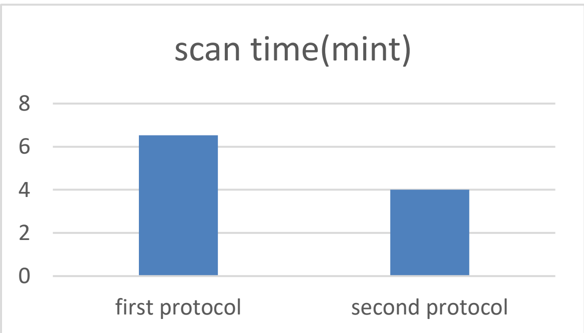

Figure 8. *Scan time for both protocols*

4. Discussion

The results demonstrated a trade-off between voxel size (spatial resolution) and the signal intensity in both T1-weighted imaging protocols with regard to the image quality. Both manual and automated measurements showed that the protocol with shorter TR and larger voxel size provided higher SNR and CNR, regardless of the measurement methods. Enhancements in signal quality are primarily due to the increase in the voxel size, which inherently contains more protons per unit volume, resulting in an improvement in signal intensity[14].

This signal gain, however, was not achieved without a loss of spatial resolution. in both Laplacian variance and entropy, the protocol with smaller voxel sizes and higher spatial resolution had better performance in edge sharpness, and the result was supported by edge strength measures for both methods. These measures relate to the ability of an image to preserve high-frequency details and textural complexity [16], both of which are important in the detection of subtle structural differences in the lumber spine.

It is expected that the smallest TR produces the best signal recovery and SNR was in fact dominated by voxel size [12]. The longer TR protocol with a smaller voxel size, however, exhibited the lower SNR, demonstrating how spatial resolution can impact signal performance in a counterintuitive way in practice. Furthermore, the manual and the automatic results also showed that the signal features of the vertebral body and the cerebrospinal fluid (CSF) were uniformly affected, indicating that the observed behavior appears to be common across different tissues.

These findings were additionally confirmed by the visual evaluation of a radiologist. Fair to good image quality and diagnostic certainty were achieved with both protocols, with the high-resolution protocol being preferred for tissue contrast. This observation has clinical relevance, as it may affect a given patient even when overall SNR and CNR measures appear unchanged. When examining the spine, where small lesions and fine anatomical margins are of diagnostic importance, the increase in the sharpness of the tissue delineation may take precedence over the increase in signal intensity.

From a time point of view, the higher resolution protocol entailed more slices and an increased number of encoding steps and, therefore, a slightly longer overall scan time. This was considered clinically acceptable by the radiologist and did not compromise diagnostic use; however, this does signal possible optimization of speed for image fidelity trade-offs.

4. Conclusion

One of the protocols had a numerical advantage in signal metrics, while the other signal protocol was superior in structural representation. This emphasizes the need to optimize MRI acquisition properties not only to maximize signal but also to maintain diagnostic detail.

Author Statements:

- **Ethical approval:** The conducted research is not related to either human or animal use.
- **Conflict of interest:** The authors declare that they have no known competing financial interests or personal relationships that could have appeared to influence the work reported in this paper
- **Acknowledgement:** The authors declare that they have nobody or no-company to acknowledge.
- **Author contributions:** The authors declare that they have equal right on this paper.
- **Funding information:** The authors declare that there is no funding to be acknowledged.
- **Data availability statement:** The data that support the findings of this study are available on request from the corresponding author. The data are not publicly available due to privacy or ethical restrictions.

References

[1] Ali, Z.., & Funjan, M. M.. (2024). Classification of Brain Infarction using Deep Learning techniques on Magnetic Resonance Imaging (MRI). *Journal of Ecohumanism*, 3(5), 92–98. https://doi.org/10.62754/joe.v3i5.3876

[2] Rashid, N. R., Al-Hilli, M., Aliasghar, A., & Shaker, Q. M. (2015). Magnetic resonance imaging of the left wrist: assessment of the bone age in a sample of healthy Iraqi adolescent males. *Journal of the Faculty of Medicine Baghdad*, 57(1), 22-26. https://doi.org/10.32007/jfacmedbagdad.571301

[3] AL-Ani, M. I., Fahed, Q. A., & Shyaa , A. I. (2023). Clinical Importance of Imaging Anatomical Signs in Predicting Transverse Sinus Dominance Using Conventional Magnetic Resonance Imaging. *Journal of the Faculty of Medicine Baghdad*, 65(1), 14-https://doi.org/10.32007/jfacmedbagdad.6511910

[4] Joori, S. M., Fadhil, A. A., Abdullateef, W. M., & Jabir, M. M. (2016). Magnetic Resonance Imaging in sonographically indeterminate adnexal masses. *Journal of the Faculty of Medicine Baghdad*, 57(4), 273-278. https://doi.org/10.32007/jfacmedbagdad.574389

Recognition, Proceedings. 15th International Conference on. 3. 314-317 vol.3. 10.1109/ICPR.2000.903548.

[5] Issa, S. Q., Mohson, khaleel I., & Fadhil, N. K. (2019). The accuracy of pelvic magnetic resonance imaging in the diagnosis of ovarian malignancy in Iraqi patients in comparison with histopathology. *Journal of the Faculty of Medicine Baghdad*, 60(4), 202-207. https://doi.org/10.32007/jfacmedbagdad.604479

[6] Joori, S. M., Albeer, M. R., & Al-Baldawi, D. S. (2013). Extraspinal incidental findings of spinal MRI. *Journal of the Faculty of Medicine Baghdad*, 55(3), 219-223. https://doi.org/10.32007/jfacmedbagdad.553618

[7] Zepeda Fernandez, C. H., Lopez Tellez, C. A., Flores Orea, Y., & Moreno Barbosa, E. (2022). Total angular momentum of water molecule and magnetic field interaction. *arXiv preprint*, arXiv:2210.01867. https://doi.org/10.48550/arXiv.2210.01867

[8] Muzamil, A., Nurdin, D. Z. I., Rohmah, J., Rulaningtyas, R., & Astuti, S. D. (2023). Cervical MRI Image Quality Optimization based on Repetition Time (TR) and Echo Train Length (ETL) Settings. *Hellenic Journal of Radiology,* 8(2). https://doi.org/10.36185/528

[9] Ginat, D. T., Fong, M. W., Tuttle, D. J., Hobbs, S. K., & Vyas, R. C. (2011). Cardiac Imaging: Part 1, MR Pulse Sequences, Imaging Planes, and Basic Anatomy. *American Journal of Roentgenology*, 197(4), 808–815. doi:10.2214/ajr.10.7231

[10] Boursianis, T.; Kalaitzakis, G.; Nikiforaki, K.; Kosteletou, E.; Antypa, D.; Gourzoulidis, G.A.; Karantanas, A.; Papadaki, E.; Simos, P.; Maris, T.G.; et al. The Significance of Echo Time in fMRI BOLD Contrast: AClinical Study during Motor and Visual Activation Tasks at 1.5 T.

[11] Strzelecki, M., Piórkowski, A., & Obuchowicz, R. (2022). Effect of Matrix Size Reduction on Textural Information in Clinical Magnetic Resonance Imaging. *Journal of Clinical Medicine*, 11(9), 2526. https://doi.org/10.3390/jcm11092526

[12] Brown, R. W., Cheng, Y.-C. N., Haacke, E. M., Thompson, M. R., & Venkatesan, R. (2014). Magnetic Resonance Imaging: Physical Principles and Sequence Design (2nd ed.). *John Wiley & Sons*. https://doi.org/10.1002/9781118633953

[13] Jackson EF, Ginsberg LE, Schomer DF, Leeds NE., (1997). A review of MRI pulse sequences and techniques in neuroimaging. *Surg Neurol.* 47(2):185-99. doi: 10.1016/s0090-3019(96)00375-8. PMID: 9040824

[14] Goerner, F. L., & Clarke, G. D. (2011). Measuring signal-to-noise ratio in partially parallel imaging MRI. *Medical Physics*, 38(9), 5049–5057. doi:10.1118/1.3618730

[15] Khunteta, A., & Ghosh, D. (2014). Edge Detection via Edge-Strength Estimation Using Fuzzy Reasoning and Optimal Threshold Selection Using Particle Swa

[16] Pech Pacheco, Jose Luis & Cristobal, Gabriel & Chamorro-Martinez, J. & Fernandez-Valdivia, J., (2000). Diatom autofocusing in brightfield microscopy: A comparative study. *Pattern*

[17] Zhai, G., & Min, X. (2020). Perceptual image quality assessment: a survey. *Science China*

Information Sciences, *63(*11). doi:10.1007/s11432-019-2757-1

[18] Plewes, D. B., & Kucharczyk, W. (2012). Physics of MRI: A primer. *Journal of Magnetic Resonance Imaging*, 35(5), 1038–1054.doi:10.1002/jmri.23642

[19] Zellers, J. A., Commean, P. K., Chen, L., Mueller, M. J., & Hastings, M. K. (2021). A limited number of slices yields comparable results to all slices in foot intrinsic muscle deterioration ratio on computed tomography and magnetic resonance imaging. *Journal of biomechanics*, 129, 110750. https://doi.org/10.1016/j.jbiomech.2021.110750

[20] Mahesh M. (2013). The Essential Physics of Medical Imaging, Third Edition. *Medical physics*, *40*(7), 10.1118/1.4811156. https://doi.org/10.1118/1.4811156